# Ultrafast photodegradation of isoxazole and isothiazolinones by UV254 and UV254/H2O2 photolysis in a microcapillary reactor

# Ultrafast photodegradation of isoxazole and isothiazolinones by $UV_{254}$ and $UV_{254}/H_2O_2$ photolysis in a microcapillary reactor

Danilo Russo[a,d*], Kristin H. Cochran[b], Danielle Westerman[b], Gianluca Li Puma[c], Raffaele Marotta[d], Roberto Andreozzi[d], Susan D. Richardson[b,*].

[a] Present address: Department of Chemical Engineering and Biotechnology, University of Cambridge, UK.

[b] Department of Chemistry and Biochemistry, University of South Carolina, USA.

[c] Environmental Nanocatalysis & Photoreaction Engineering, Department of Chemical Engineering, Loughborough University, UK.

[d] Dipartimento di Ingegneria Chimica, dei Materiali e della Produzione Industriale, Università di Napoli Federico II, Italy.

*Corresponding author: Danilo Russo: danilo.russo3@unina.it; dr473@cam.ac.uk; Susan D. Richardson, RICHA545@mailbox.sc.edu.

Keywords: micropollutants; advanced oxidation processes; isoxazole; water reclamation; water treatment; isothiazolinones.

*Highlights*

- $H_2O_2/UV_{254}$ and $UV_{254}$ for the removal of isothiazolinones and isoxazole
- A convenient ultrafast microcapillary photoreactor was adopted for AOP studies
- Photokinetic parameters of target isothiazolinones and isoxazole were estimated
- The main oxidized BIT transformation products were tentatively identified
- A novel mechanistic degradation pathway was proposed for BIT

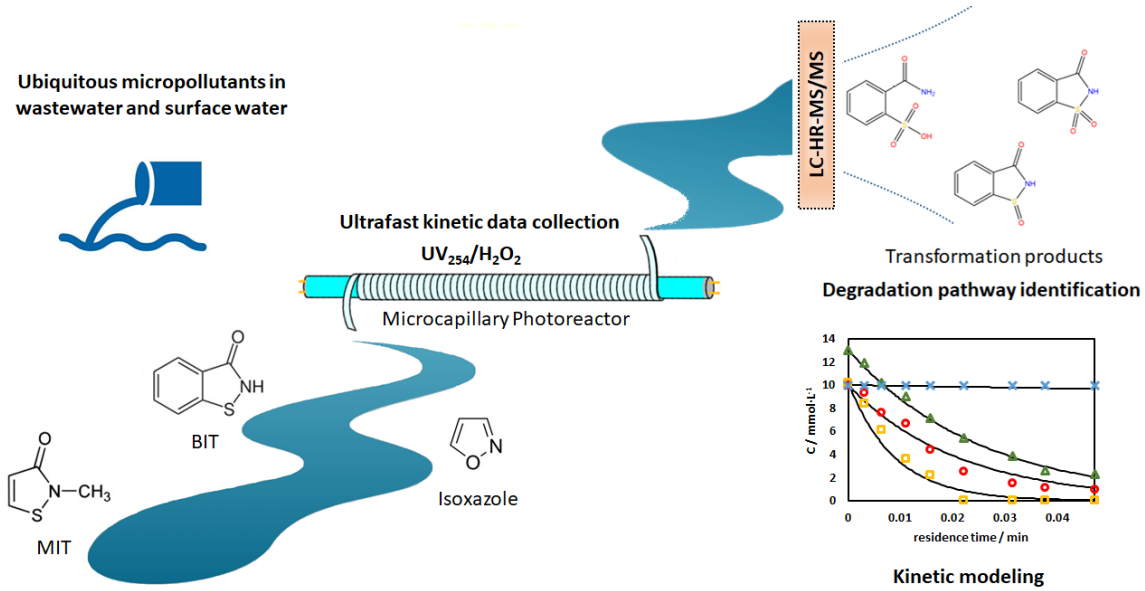


## Abstract

The photodegradation process of methylisothiazolinone (MIT), benzisothiazolinone (BIT), and isoxazole (ISOX) in ultrapure water and synthetic wastewater by means of $UV_{254}$ photolysis and by $UV_{254}/H_2O_2$ advanced oxidation process were investigated in a microcapillary photoreactor designed for ultrafast photochemical transformation of microcontaminants. For the first time, we estimated key photo-kinetic parameters, i.e. quantum yields (35.4 $mmol \cdot ein^{-1}$ for MIT, and 13.5 and 55.8 $mmol \cdot ein^{-1}$ for BIT at pH = 4-6 and 8, respectively) and rate constants of the reaction of photo-generated OH radicals with MIT and BIT ($2.09 \cdot 10^9$ and $5.9 \cdot 10^9$ $L \cdot mol^{-1} \cdot s^{-1}$ for MIT and BIT). The rate constants of the reaction of photo-generated OH radicals with ISOX in MilliQ water was also estimated $2.15 \cdot 10^9$ $L \cdot mol^{-1} \cdot s^{-1}$) and it was in good agreement with literature indications obtained in different aqueous matrices. The models were extended and validated to the case of simultaneous degradation of mixtures of these compounds and using synthetic wastewater as an aqueous matrix. High resolution-accurate mass mass spectrometry analysis enabled identification of the main intermediates (BIT200, B200, saccharin, BIT166) and enabled proposal of a novel degradation pathway for BIT under $UV_{254}/H_2O_2$ treatment. This study demonstrates an ultrafast method to determine key photo-

kinetic parameters of contaminants of emerging concern in water and wastewater, which are needed for design and validation of photochemical water treatment processes of municipal and industrial wastewaters.

## 1. Introduction

Isoxazole and isothiazolinones are five-membered heterocyclic compounds having various pharmacological and antimicrobial properties (Hamada et al., 2011; Lee et al., 2002; Clerici et al., 2008). The large interest in these substances and their derivatives is due to their versatility as synthetic building blocks (Gribble et al., 2003). As a result of their massive adoption in a wide variety of commonly used products, such compounds have been included in the class of emerging pollutants (Ghattas et al., 2017; Shi et al., 2012). The current broad definition of emerging pollutants includes a significant number of chemicals normally employed in detergents, personal care products, pharmaceuticals and drugs, which are usually present in wastewater and surface water at levels from ng to μg per liter (Miraji et al., 2016; Wanda et al., 2017; McCance et al., 2018; Guo et al., 2018). Despite their low levels, their potential ecotoxicological effect cannot be ruled out (Kohanski et al., 2010; Lin et al., 2010) and several studies addressed the problem of their removal from liquid and solid compartments (Stamm et al., 2015; Bollmann et al., 2017; Luo et al., 2014, Margot et al., 2015).

2-Methyl-1,2-thiazol-3(2H)-one, also named methylisothiazolinone (MIT), and 1,2-Benzisothiazol-3(2H)-one, or benzisothiazolinone (BIT), are very common biocides employed in personal care products, detergents (Li et al., 2016a; Garcia-Hidalgo et al., 2016), roof and outdoor paints, paper materials, and in other important industrial applications (Jungnickel et al., 2008; Wieck et al., 2016, Wang et al., 2017; Li et al., 2016b), i.e. in reverse osmosis processes for water reclamation and desalination (Li et al., 2016a) and, in high concentrations, in cooling towers, paper mills, and refinery industry (Amat et al., 2015). As a result, significant

69 concentrations of MIT and BIT have been reported in wastewater treatment plants' (WWTPs')
70 influent, effluent, and in surface water (Wieck et al., 2016; Speksnijder et al., 2010; Zhang et
71 al., 2015; Liu et al., 2015). The potential impact of MIT and BIT to the aquatic environment
72 and humans is addressed by several studies (Li et al., 2016a; Van Huizen et al., 2017; Li et al.,
73 2016b; Lugg, 2001; Geier et al., 2012). MIT was named allergen of the year IN 2013 (Van
74 Huizen et al., 2017). The biocidal effect of MIT also affects the efficiency of activated sludge
75 in wastewater treatment and as a result, the efficiency of the nitrification process can decrease
76 from 90 to 20 % (Amat et al., 2015).
77 Previous studies show slow degradation of MIT by divalent ferric ions (Tanji et al., 2007),
78 $TiO_2$, and ZnO based photocatalysis under UV irradiation (Kandavelu et al., 2004), and by
79 electrochemical methods (Han et al., 2011). Ozonation was found to be effective in the
80 degradation of first- and second- generation by-products of both MIT and BIT and in the
81 reduction of treated sample ecotoxicity for longer treatment times (Li et al., 2016a, Li et al.,
82 2016b), whereas studies on BIT degradation in water under UV-C irradiation were recently
83 conducted by Wang et al., (2017).
84 Isoxazole (ISOX) derivatives are commonly used in different pharmaceuticals as antifungal
85 (Vicentini et al., 2011), anticancer (Yong et al., 2015), anti-HIV (Srivastava et al., 1999), and
86 ulcerogenic (Daidone et al., 1999) agents. Some isoxazole derivatives have antibiotic activity;
87 a typical case is sulfamethoxazole, an antibiotic used worldwide, and prescribed for treatment
88 of urinary infections.
89 Isoxazole-based compounds are also employed as COX-2 inhibitors and anti-inflammatory
90 drugs (Zimecki et al., 2018; Maczynski et al., 2016). Some isoxazole derivatives were detected
91 in different sewage treatment plant effluents, surface waters and drinking waters at low $ng \cdot L^{-1}$
92 levels (Schriks et al., 2010; Andreozzi et al., 2003; Hirsch et al., 1999).

Advanced oxidation processes (AOPs) have been widely adopted for the successful degradation of a wide range of emerging pollutants. Specifically, UV/$H_2O_2$ offers several advantages, including easy operation, reduced costs and high removal efficiency for both parent compounds and their transformation products (Bensalah et al., 2018; Huang et al., 2018; Li et al., 2007), resulting also in a decrease of the ecotoxicological effects of processed solutions for well-designed treatment times (Siciliano et al., 2018).

In this study, the degradation of MIT, BIT, and isoxazole (Fig. 1) was studied under $UV_{254nm}$ and $UV_{254nm}/H_2O_2$ in ultrapure MilliQ water in order to estimate the main kinetic parameters, such as direct photolysis quantum yields and the rate constants of the reaction of photo-generated OH radicals and these emerging pollutants.

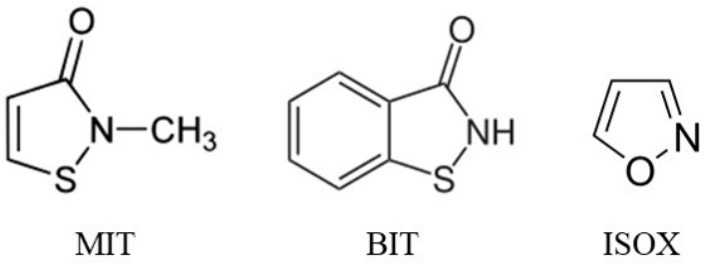


MIT BIT ISOX

**Fig. 1.** Structural formulas for MIT, BIT, and ISOX.

Kinetic experiments were carried out in MilliQ and synthetic wastewater using a microcapillary photo-reactor (Reis and Li Puma, 2015) and were kinetically modelled using previous approaches (Russo et al., 2017). The adoption of this microreactor enabled collection of several experimental samples in a simple, safe, and fast experimental campaign, reducing reaction times, waste solution volumes, and costs associated with the adoption of batch-scale quartz and glass reactors, high power lamps, waste disposal, and expensive reagents.

In addition to kinetic experiments, treated and untreated solutions were analyzed via high resolution-accurate mass mass spectrometry to identify the primary oxidation/degradation products of the three contaminants of interest (MIT, BIT, and ISOX).

A novel mechanistic pathway was proposed for BIT utilizing one of two common addition mechanisms known in sulfur chemistry (Atkinson et al., 1997, Barnes et al., 1996, Wine et al., 1981, Hynes and Wine et al., 1995). Oxidation of sulfur-containing compounds often adds oxygen to the sulfur heteroatom, which can somewhat uniquely contain 2, 4, or 6 bonds, through either (i) hydrogen abstraction or (ii) radical addition (Atkinson et al., 1997, Wine et al., 1981; Barnes et al., 1996). Hydrogen abstraction commonly happens when the sulfur heteroatom is adjacent to a methyl or C-H-containing group, where the hydroxyl radical pulls a hydrogen off to form water and an analyte radical; as BIT's sulfur is adjacent to an amide group, this mechanism is unlikely for BIT advanced oxidation (Atkinson et al., 1997; Barnes et al., 1996). The more likely mechanism is radical addition through direct attack of the hydroxyl radical on the sulfur heteroatom and further oxidation by oxygen ($O_2$) present in the reactor water (Hynes et al., ; Wine et al., 1981). Hydroxyl radicals ($^{\bullet}OH$) are generated from ultraviolet (UV) treatment of hydrogen peroxide ($H_2O_2$) and subsequently react with the analyte (Atkinson et al., 1997).

To the best of our knowledge, this is the first study investigating the photodegradation of the target compounds by $UV_{254}$ and $UV_{254}/H_2O_2$ processes by ultrafast sample generation, laying the groundwork for future investigations on the removal efficiency in real wastewater matrices and ecotoxicity studies of the treated and untreated compounds on aquatic life. This is also the first $UV/H_2O_2$ advanced oxidation degradation pathway proposed for BIT.

## 2. Materials and Methods

### 2.1. Materials

2-Methyl-4-isothiazolin-3-one (98%), 1,2-benzisothiazol-3(2H)-one (98%), isoxazone (99%), sulfuric acid (1 N), NaOH (97%), NaCl (99.5%), $CaCl_2$ (99%), meat extract, peptone microbiology grade, urea (98%), $K_2HPO_4$ (98%), $Mg_2SO_4$ (99%), hydrogen peroxide solution (35%), benzoic acid (99.5%), methanol (99.99%), and acetonitrile (99.99%) were purchased from Sigma-Aldrich.

Synthetic wastewater was prepared by adding peptone (32 $mg \cdot L^{-1}$), meat extract (22 $mg \cdot L^{-1}$), urea (6 $mg \cdot L^{-1}$), $K_2HPO_4$ (28 $mg \cdot L^{-1}$), $CaCl_2$ (4 $mg \cdot L^{-1}$), NaCl (7 $mg \cdot L^{-1}$), $MgSO_4$ (0.6 $mg \cdot L^{-1}$) to MilliQ water in accordance with OECD guidelines (Organisation for Economic Cooperation and Development, 1999) and stored at 4 °C for less than 24 h. pH was adjusted using diluted solutions of sulfuric acid and sodium hydroxide. No significant pH variations were detected during the experiments.

## 2.2. Continuous flow experiments

The experimental setup has been described in detail elsewhere (Reis and Li Puma, 2015; Russo et al., 2016). Briefly, it consists of a fluoropolymer flat strip containing 10 microcapillaries with a mean diameter of 195 μm, wrapped around a monochromatic (254 nm) germicidal lamp (Germicidal G8T5). The nominal power supplied to the lamp could be varied from 8 W to 4.5 W using a variable power supplier. The photonic power per unit reactor volume $\left(\frac{I_{254}}{V}\right)$ emitted were estimated by hydrogen peroxide actinometry (Nicole et al., 1990) and were $1.92 \cdot 10^{-2}$ $ein \cdot s^{-1} \cdot L^{-1}$ and $1.27 \cdot 10^{-2}$ $ein \cdot s^{-1} \cdot L^{-1}$, respectively (Russo et al., 2017). The adopted flow rates through the microcapillary photoreactor were in the range 0.6 – 1 $mL \cdot min^{-1}$. The fluid residence time (i.e. space time) was varied changing both the flowrate and the length of the reactor exposed to the $UV_{254}$ radiation. Previously reported tracer experiments showed a fluid-dynamic behaviour approaching plug-flow. In a typical experiment, the reactor was washed with MilliQ water. The lamp was turned on for the same amount of time to reach stationary conditions

before adding the MIT, BIT, or ISOX to the feed tank. Samples were collected directly into vials at the outlet of the reactor and analyzed using a spectrophotometer and a high-performance liquid chromatograph (HPLC). The reactor was always operated in single pass without any recirculation of the solutions. Preliminary experiments showed that the solutions were not reactive under dark conditions.

### 2.3. Analytical methods

Absorbance spectra at 254 nm were acquired using a PerkinElmer Lambda 35 UV/Vis spectrometer.

Chromatographic analysis was carried out using an Agilent 1100 HPLC equipped with a Restek Ultra C18 LC column (250 x 4.60 mm 5 μm) and a DAD detector. The column was maintained at 30 °C. The mobile phase consisted of 8% aqueous methanol, 18% aqueous acetonitrile, and 6% aqueous MeOH for MIT, BIT, and ISOX, respectively. Retention times were 2.3, 12.3, and 8.1 min, respectively.

Samples containing 10 parts per million ($mg \cdot L^{-1}$) of BIT, MIT, and ISOX reacted with $UV_{254}/H_2O_2$ were loaded on solid phase extraction (SPE) cartridges and kept frozen until analysis. SPE cartridges were eluted with 15 mL 50:50 methanol:acetone, evaporated to 500 μL under nitrogen, and a fraction (200 μL) was diluted with purified water and analyzed by LC-mass spectrometry (MS)/MS for transformation product (TP) identification.

Transformation products (TPs) of BIT, MIT, and ISOX were analyzed by an Agilent 6545 ultra-high-performance liquid chromatograph (UHPLC) quadrupole-time-of-flight (QTOF) mass spectrometer with a Poroshell C18 UHPLC column (2.1 mm × 150 mm × 2.7 μm, Agilent InfinityLab). Electrospray ionization (ESI) was used in both positive and negative ion mode. The LC mobile phase consisted of water and methanol, containing 0.1% formic acid and 5 mM ammonium acetate, with a flow of 0.5 $mL \cdot min^{-1}$ and an injection volume of 10 μL. A gradient

elution was used: 70% water/30% methanol, held for one min, then ramped to 2% water/98% methanol over 9 min, and returned to initial conditions over 2 min. The mass spectrometer was operated at a fragmentation voltage of 110 V, capillary voltage of 4000 V, gas temperature of 300°C, drying gas of 12 $L \cdot min^{-1}$, and nebulizer pressure of 35 psi. The scan range was from m/z 50 to 750, and collision energy for MS/MS analyses was 30 eV.

## 3. Results

### *3.1. Absorbance spectra*

Absorption spectra of the three investigated compounds are reported in Fig. 2 in the range 200-400 nm at different pH. However, it is worth noting that at 254 nm, the molar extinction coefficients of MIT at different pH are similar, whereas no significant absorbance of ISOX solution could be detected. The estimated molar extinction coefficients of MIT and BIT are summarized in Table 1.

**Table 1.** Molar absorption coefficients of MIT and BIT at 254 nm.

| Compound | ε (pH 4-6) / $L \cdot mmol^{-1} \cdot cm^{-1}$ | ε (pH 8) / $L \cdot mmol^{-1} \cdot cm^{-1}$ |
|---|---|---|
| MIT | 4.76 | 5.40 |
| BIT | 3.20 | 3.65 |

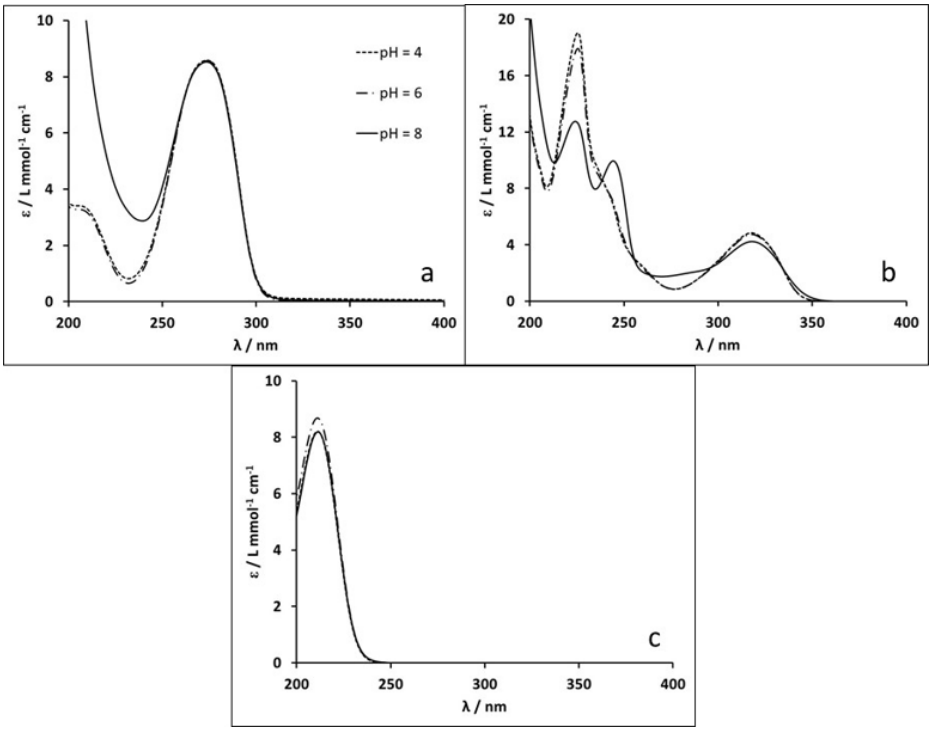


**Fig. 2.** Absorbance spectra for MIT (a), BIT (b), and ISOX (c) at different pH.

*3.2. Direct photolysis in MilliQ water: estimation of quantum yields of direct photolysis*

The quantum yields of MIT, BIT and ISOX under direct photolysis in MilliQ water was determined for the experimental conditions summarized in Table S1. The data were modeled according to the kinetic model previously reported (Russo et al., 2016; Russo et al., 2018). The kinetics of photodegradation of the compound $[S_i]$ occurs in accordance to the following modeling equation:

$$\frac{d[S_i]}{dt} = -\frac{I_{254}}{V} \cdot \Phi_{254}^{S_i} \cdot \left(1 - \exp\left(-2.3 \cdot l \cdot \varepsilon_{254}^{S_i} \cdot [S_i]\right)\right) \quad (1)$$

where $\frac{I_{254}}{V}$ is the estimated photonic power per unit reactor volume, $\Phi_{254}^{S^i}$ is the quantum yield of direct photolysis, $l$ = 152 μm is the mean optical length of the microcapillary photoreactor (Russo et al., 2016), and $\varepsilon_{254}^{S_i}$ the molar absorption coefficient of the reacting species at 254 nm (Table 1). Eq. 1 was fitted to the results of the experiments reported in Table S1 and the quantum yield $\Phi_{254}^{S^i}$ of each reacting species was determined by minimizing the overall mean

square error between the experimental and the calculated data, using an optimization routine in Matlab software (optimization mode). Fig. 3 shows the prediction of the model and the experimental data for some of the adopted conditions. All the experiments used for the modelling were reported in the Supplementary Information (Fig. S1, Table S1). The quantum yield of direct photolysis for BIT was found to be pH dependent, in agreement with the fact that also the absorbance at 254 nm is a function of pH (Section 3.1). Specifically, BIT degradation was faster at pH 8. The estimated values were summarized in Table 2, together with their 97% intervals of confidence. As shown in Fig. 3.C, ISOX does not undergo direct photolysis at 254 nm since does not absorbs at this wavelength (Fig.2). The adopted model is able to predict the degradation of MIT and BIT under direct photolysis and under different experimental conditions (initial concentration, pH and photon fluxes).

**Table 2.** Estimated quantum yields.

| Compound | $\Phi_{254}^{pH=4-6}(mmol \cdot ein^{-1})$ | $\Phi_{254}^{pH=8}(mmol \cdot ein^{-1})$ |
|---|---|---|
| MIT | 35.42 ± 0.88 | |
| BIT | 13.45 ± 0.52 | 55.80 ± 1.33 |

.

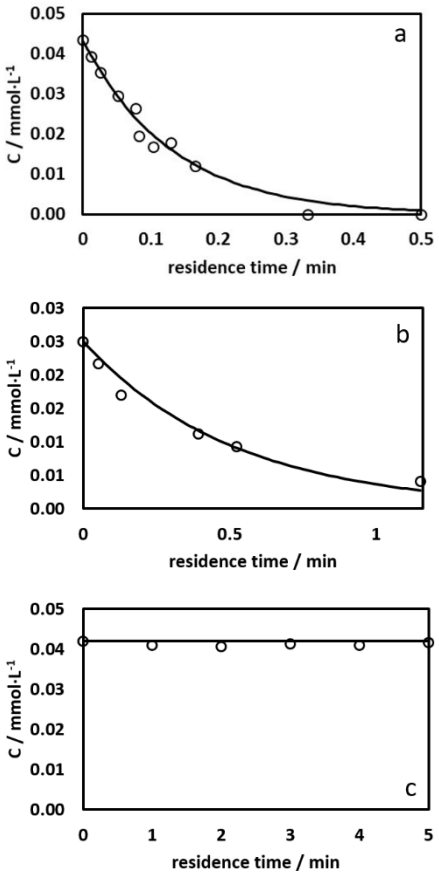


231

232 Fig. 3. Direct photolysis of MIT (a), BIT (b), and ISOX (c) at pH = 6 and nominal P = 8.0 W.

233 Experimental data (○), calculated data (curves). a) $[MIT]_0$ = 0.0434 mmol·$L^{-1}$. b) $[BIT]_0$ =

234 0.0434 mmol·$L^{-1}$. c) $[ISOX]_0$ = 0.0420 mmol·$L^{-1}$.

235

236 *3.3. $UV_{254}/H_2O_2$ treatment in MilliQ water: $k_{HO}$ estimation*

237 The reaction of MIT, BIT, and ISOX under $UV_{254}$ and in the presence of $H_2O_2$ in MilliQ water

238 was further investigated to determine the second-order kinetic rate constant of reaction of the

239 target compounds with photogenerated HO radicals $\left(k_{HO}^{i}\right)$ generated by the photolysis of $H_2O_2$.

240 The experimental data were modeled according to the modeling equations (2-5) and the $k_{HO}^{i}$

241 was determined by minimizing the mean squared error between calculated and experimental

242 data. A detailed derivation of eq. 2-5, together with the adopted simplyfing assumptions can be

243 found in (Spasiano et al., 2016a). Briefly, it was assumed that the parent compound and all

reaction products react with photogenerated HO radicals with the same kinetic rate constant $k_{HO}^{i}$ and that the sum of their concentrations is always equal to the initial concentration of the target compound $[S_i]_0$.

$$\frac{d[H_2O_2]}{dt} = -F_{H_2O_2} - \frac{F_{H_2O_2} \cdot k_H \cdot [H_2O_2]}{k_{HO}^{i}[S_i]_0 + k_H[H_2O_2]} \quad (2)$$

$$\frac{d[S_i]}{dt} = -\frac{I_{254}}{V}\Phi_{254}^{S_i}(1 - \exp(-2.3 \cdot l \cdot A_{tot}))\frac{\varepsilon_{254}^{S_i} \cdot [S_i]}{A_{tot}} - \frac{2k_{HO}^{i}[S_i]F_{H_2O_2}}{k_{HO}^{i}[S_i]_0 + k_H[H_2O_2]} \quad (3)$$

where

$$F_{H_2O_2} = \frac{I_{254}}{V}\Phi_{254}^{H_2O_2}(1 - \exp(-2.3 \cdot l \cdot A_{tot})) \cdot \frac{\varepsilon_{254}^{H_2O_2} \cdot [H_2O_2]}{A_{tot}} \quad (4)$$

$$A_{tot} = \varepsilon_{254}^{H_2O_2} \cdot [H_2O_2] + \varepsilon_{254}^{S_i} \cdot [S_i] \quad (5)$$

where $k_H$ ($2.7 \cdot 10^7$ L·mol$^{-1}$·s$^{-1}$) is the rate constant for the reaction between HO radicals and hydrogen peroxide, $\Phi_{254}^{H_2O_2}$ (0.55 mol·ein$^{-1}$) is the quantum yield for direct photolysis of hydrogen peroxide at 254 nm, and $\varepsilon_{254}^{H_2O_2}$ (18.6 L·mol$^{-1}$·cm$^{-1}$) is the molar absorption coefficient of hydrogen peroxide (Russo et al., 2016; Spasiano et al., 2016a). The adopted experimental conditions are summarized in Table S2. The comparisons between the experimental and calculated concentrations for hydrogen peroxide and the target compounds for all the adopted conditions are reported in Fig. 2S A-C whereas Fig. 4 shows the results only for a few explicative examples.

The best estimated values of $k_{HO}^{i}$ together with their 97% confidence intervals are summarized in Table 3. The estimated value for ISOX is in good agreement with the one previously reported in the literature ($3.5 \cdot 10^9$ L·mol$^{-1}$·s$^{-1}$) (Dogan et al., 1990). The discrepancy can be ascribed to the interference of other compounds in the water matrix adopted in the previous study. It is woth noticing that ISOX and MIT have very similar rate constant. This can be explained considering that they have very similar structure and they might undergo H abstraction by OH

radicals as previously reported for ISOX (Dogan et al., 1990). On the other hand, the higher value of the rate constant estimated for BIT is in good agreement with those reported for heterocyclic aromatics, for which the aromatic ring hydroxylation is more likely to occur (Sagi et al., 2015).

Competition kinetics with benzoic acid as a reference compound were also used to estimate the value of $k_{HO}^{ISOX}$, since it is reported that this method gives a good estimate of the rate constant when the organic compounds do not undergo direct photolysis or tha latter is negligible (Spasiano et al., 2016a). The estimated value of $k_{HO}^{ISOX}$ was $3.0 \cdot 10^9$ $L \cdot mol^{-1} \cdot s^{-1}$, in good agreement with the one reported in Table 3. The slight discrepancies between the two methods have been already observed for other compounds (Spasiano et al., 2016a; Spasiano et al., 2016b; Russo et al., 2017; Russo et al., 2018; Garcia Einschlag et al., 2003).

**Table 3.** Estimated $k_{HO}^{i}$ values for the investigated compounds.

| Compound | $k_{HO}^{i}(L \cdot mol^{-1} \cdot s^{-1})$ |
|---|---|
| MIT | $(2.09 \pm 0.21) \cdot 10^9$ |
| BIT | $(5.90 \pm 0.69) \cdot 10^9$ |
| ISOX | $(2.15 \pm 0.12) \cdot 10^9$ |

.

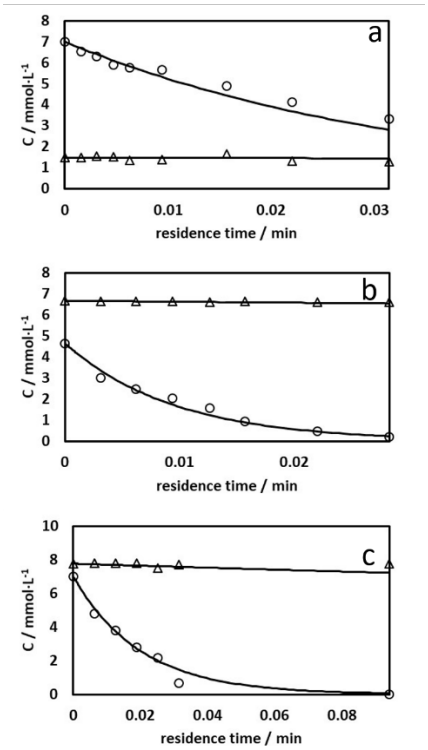


278

279 **Fig. 4.** Photodegradation of MIT (a), BIT (b), and ISOX (c) by $UV_{254}/H_2O_2$.in MilliQ water
280 at pH = 6 and nominal P = 8.0 W: experimental data (symbols), calculated data (lines).
281 organics (○), $H_2O_2$ (Δ). BIT concentrations are multiplied by 160 for viewing convenience. a)
282 $[MIT]_0 = 0.044$ mmol·L$^{-1}$; $[H_2O_2]_0 = 1.48$ mmol·L$^{-1}$. b) $[BIT]_0 = 0.029$ mmol·L$^{-1}$; $[H_2O_2]_0 =$
283 6.68 mmol·L$^{-1}$. c) $[MIT]_0 = 0.040$ mmol·L$^{-1}$; $[H_2O_2]_0 = 7.77$ mmol·L$^{-1}$.

284

285 *3.4. $UV_{254}/H_2O_2$ treatment in synthetic wastewater*

286 Most photodegradation treatment processes take place in real wastewater plants in which a
287 considerable number of other compounds are present. The effect of the water matrix on the
288 system can be complex (Lado Ribeiro et al., 2019) because compounds like nitrates can be an
289 additional source of hydroxyl radical (Mack and Bolton, 1999). However, most photo-
290 degradation kinetics can be successfully modeled, taking into account naturally occuring
291 compounds that act as scavengers for hydroxyl radicals, which decrease the degradation
292 efficiency for target compounds (Spasiano et al., 2016a). In this case, the modeling equations

(eq. 6-9) can be modified, taking into account the absorbance of the real aqueous matrix and introducing a scavenging term $k_{sca}$ as follows:

$$\frac{d[H_2O_2]}{dt} = -F_{H_2O_2} - \frac{F_{H_2O_2} \cdot k_H \cdot [H_2O_2]}{k_{HO}^i[S_i]_0 + k_H[H_2O_2] + k_{sca}} \quad (6)$$

$$\frac{d[S_i]}{dt} = -\frac{I_{254}}{V}\Phi_{254}^{S_i}(1 - \exp(-2.3 \cdot l \cdot A_{tot}))\frac{\varepsilon_{254}^{S_i} \cdot [S_i]}{A_{tot}} - \frac{2k_{HO}^i[S_i]F_{H_2O_2}}{k_{HO}^i[S_i]_0 + k_H[H_2O_2] + k_{sca}} \quad (7)$$

where

$$F_{H_2O_2} = \frac{I_{254}}{V}\Phi_{254}^{H_2O_2}(1 - \exp(-2.3 \cdot l \cdot A_{tot})) \cdot \frac{\varepsilon_{254}^{H_2O_2} \cdot [H_2O_2]}{A_{tot}} \quad (8)$$

$$A_{tot} = \varepsilon_{254}^{H_2O_2} \cdot [H_2O_2] + \varepsilon_{254}^{S_i} \cdot [S_i] + A_{matrix} \quad (9)$$

and where $A_{matrix}$ is the total absorbance at 254 nm of the synthetic aqueous matrix, which often may be considerably negligible with respect to the absorbance of hydrogen peroxide and the aromatic compounds. As reported by Spasiano et al., 2016a, $k_{sca} = k'[SCA]$, where $k'$ is the kinetic rate constant of the reaction between OH radicals and the scavengers species ($SCA$). As a result, it can be considered as a constant for a selected aqueous matrix assuming that the concentration of the scavengers $[SCA]$ is much greater than the one of the polluttants. To further support this point and validate previous models (Sections 3.2 and 3.3) and the kinetic parameters estimated in this work, kinetic experiments were carried out by dissolving the target compounds in synthetic wastewater prepared according to the OECD guidelines as specified in Section 2.1. Equations 6-9 were simultaneously solved for the chosen experimental conditions using the previously estimated value for the $k_{sca}$ ($4.01 \cdot 10^5$ $s^{-1}$) (Spasiano et al., 2016a; Russo et al., 2017) without any further adjustement of any of the previously estimated kinetic parameters (simulation mode). As shown in Fig. 5, the model is still capable of predicting degradation of the target compounds by $UV_{254}/H_2O_2$ in synthetic wastewaters.

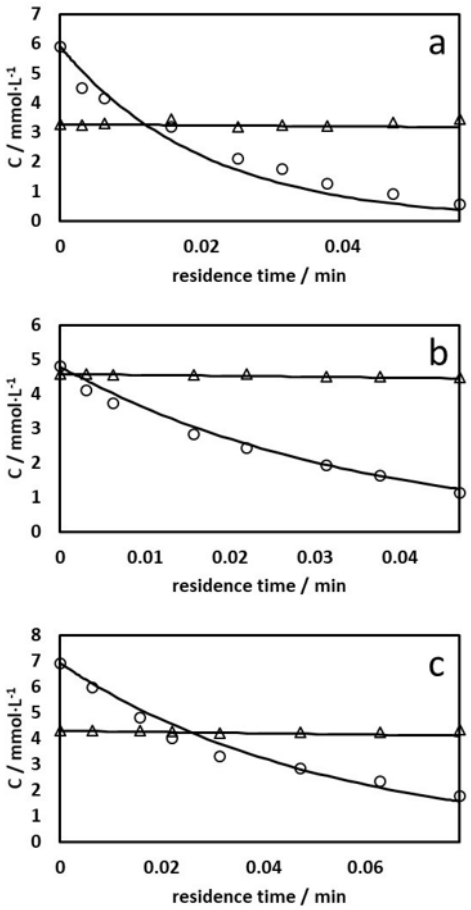


311

312 **Fig. 5.** Degradation of (a) MIT; (b) BIT; (c) ISOX by UV/$H_2O_2$ in synthetic wastewater.
313 Pollutant (○) , $H_2O_2$ (Δ). Pollutant concentrations are multiplied by 160 for viewing
314 convenience. (a) $[S_i]_0$ = 0.037 mM, $[H_2O_2]_0$ = 3.28 mM, overall σ(%) = 2.16; (b) $[S^i]_0$ =
315 0.030 mM, $[H_2O_2]_0$ = 4.58 mM, overall σ(%) = 0.85; (c) $[S_i]_0$ = 0.043 mM, $[H_2O_2]_0$ = 4.30
316 mM, overall σ(%) = 2.45; pH=6.0; P = 8 W.

317 *3.5. Mixture of MIT, BIT, and ISOX in MilliQ water*

318 Mixtures of MIT, BIT, and ISOX in MilliQ water were further irradiated with $UV_{254}$ only and
319 in the presence of $H_2O_2$ to validate the model and the level of confidence of the quantum yields
320 and OH rate constants for the three species reported in Tables 2 and 3. The direct photolysis of
321 the mixture with $UV_{254}$, can be modeled using eq. (1) modified for the absorption of the three
322 species as shown in eq. (10):

$$\frac{d[S_i]}{dt} = -\frac{I_{254}}{V} \cdot \Phi_{254}^{S_i} \cdot \left(1 - \exp\left(-2.3 \cdot l \cdot \sum_i \varepsilon_{254}^{S_i} \cdot [S_i]\right)\right) \cdot \frac{\varepsilon_{254}^{S_i} \cdot [S_i]}{\sum_i \varepsilon_{254}^{S_i} \cdot [S_i]} \quad (10)$$

assuming that the interaction of the photogenerated by-products with their parent compounds negligibly affected their degradation. This assumption was partially corroborated by the experimental evidence that ISOX concentration profiles were invariant under the adopted conditions. Results of the simulation without any further adjustment of the previous estimated kinetic parameters are reported in Fig. 6 a-b (simulation mode). The same procedure was applied in the presence of hydrogen peroxide ($UV_{254}/H_2O_2$), modifying the kinetics as follows (eq. 11-14). The results of the simulations are reported in Fig. 6 c-d.

$$\frac{d[H_2O_2]}{dt} = -F_{H_2O_2} - \frac{F_{H_2O_2} \cdot k_H \cdot [H_2O_2]}{\sum_i k_{HO}^i [S_i]_0 + k_H [H_2O_2]} \quad (11)$$

$$\frac{d[S_i]}{dt} = -\frac{I_{254}}{V} \Phi_{254}^{S_i} (1 - \exp(-2.3 \cdot l \cdot A_{tot})) \frac{\varepsilon_{254}^{S_i} \cdot [S_i]}{A_{tot}} - \frac{2k_{HO}^i [S_i] F_{H_2O_2}}{\sum_i k_{HO}^i [S_i]_0 + k_H [H_2O_2]} \quad (12)$$

where

$$F_{H_2O_2} = \frac{I_{254}}{V} \Phi_{254}^{H_2O_2} (1 - \exp(-2.3 \cdot l \cdot A_{tot})) \cdot \frac{\varepsilon_{254}^{H_2O_2} \cdot [H_2O_2]}{A_{tot}} \quad (13)$$

$$A_{tot} = \varepsilon_{254}^{H_2O_2} \cdot [H_2O_2] + \sum_i \varepsilon_{254}^{S_i} \cdot [S_i] \quad (14)$$

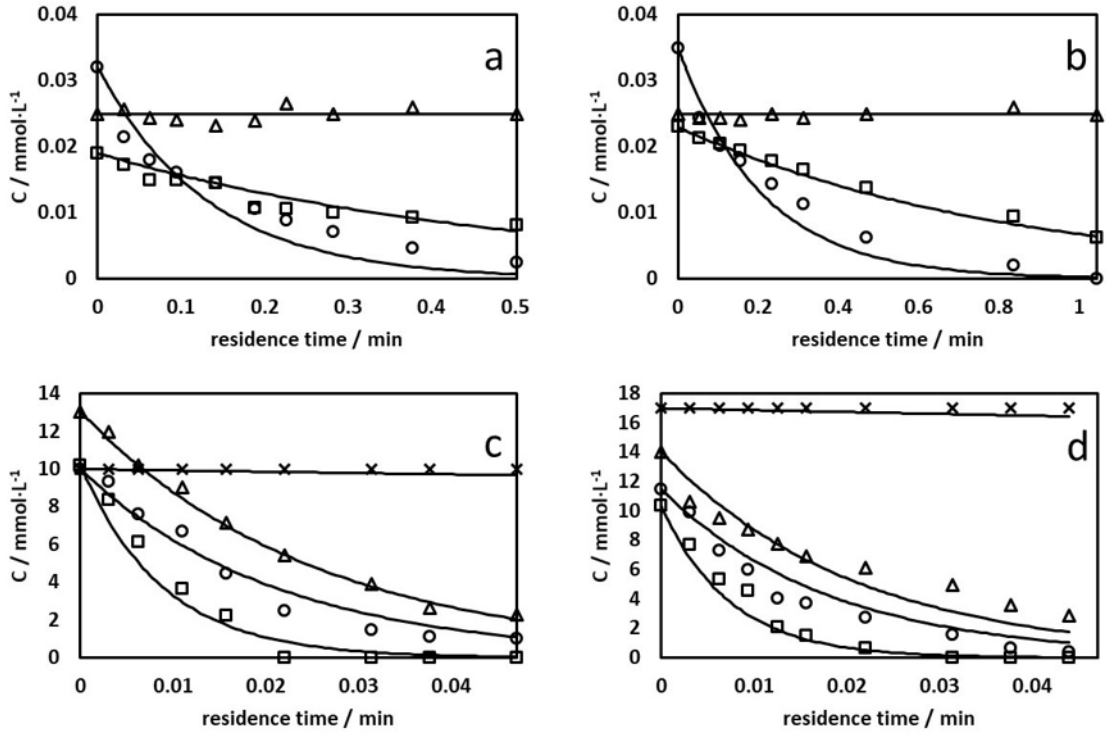


**Fig. 6.** Photodegradation of mixtures of MIT, BIT, and ISOX using $UV_{254}$ (a,b) and $UV_{254}/H_2O_2$ (c,d) in MilliQ water at pH = 6.0. (a): $[MIT]_0$ = 0.032 mM, $[BIT]_0$ = 0.019 mM, $[ISOX]_0$ = 0.025 mM, P = 8.0 W; (b): $[MIT]_0$ = 0.035 mM, $[BIT]_0$ = 0.023 mM, $[ISOX]_0$ = 0.025 mM, P = 4.5 W; (c): $[MIT]_0$ = 0.020 mM, $[BIT]_0$ = 0.020 mM, $[ISOX]_0$ = 0.026 mM, $[H_2O_2]_0$ = 10 mM, P = 8.0 W; (d): $[MIT]_0$ = 0.023 mM, $[BIT]_0$ = 0.021 mM, $[ISOX]_0$ = 0.028 mM, $[H_2O_2]_0$ = 17 mM, P = 4.5 W. (○) MIT; (□) BIT; (Δ) ISOX; (x) $H_2O_2$.

*3.6. Transformation product identification*

Several $UV_{254}/H_2O_2$ TPs of BIT were tentatively identified using UHPLC–high resolution–accurate mass-tandem spectrometry (UHPLC-HR-MS/MS). No TPs of MIT or ISOX were observed by UHPLC-MS/MS, despite their rapid degradation. This is likely due to either mineralization of these molecules or degradation to small molecules that are not amenable to electrospray ionization. Based on the observed TPs, the most likely pathway of degradation of BIT is radical addition of oxygen to the heterocyclic ring.

A mechanistic pathway for BIT degradation via UV/$H_2O_2$ advanced oxidation has been proposed (Fig. 7). Hydroxyl radical formation is catalyzed via reaction of ultraviolet light with hydrogen peroxide; the resulting radicals, along with $O_2$ in the non-degassed water reacted with BIT to form several transformation products. Based on reaction rates in literature for dimethyl sulfide (DMS), dimethyl sulfoxide, and dimethyl sulfone (Atkinson et al., 1997), the rates of steps including unobserved intermediates are expected to be very fast, which is likely the reason the intermediates weren't seen via mass spectrometry. Partial pressure of $O_2$ is also known to affect reaction rates (Ramirez-Anguita et al., 2008).

BIT reacts first with hydroxyl radicals to form hydroxylated BIT (BIT-OH), a fast intermediate that oxidizes further via $O_2$ in the reactor water to form BIT166 (BIT Sulfoxide (BIT-SO)). BIT166 is the first observed TP, with addition of one oxygen to the sulfur heteroatom. The observed accurate mass ($[M-H]^-$: m/z 165.9965, $C_7H_5O_2NS$) is within 2.0 ppm of the theoretical mass. The fragmentation (m/z 134.0249 and m/z 122.9914) observed also supports the proposed structure, corresponding to loss of sulfur (m/z 134.0249) and loss of an amide (m/z 122.9914), respectively, both likely through rearrangement. While loss of sulfur is unusual, there is supporting evidence from the National Institute of Standards and Technology (NIST) library of this occurring in a similar structure, dibenzothiophene 5-oxide, which also has a ring-bound sulfoxide group, as well as MS/MS evidence of this specific product loss from a prior ozonation study conducted by Li et al. (Li et al., 2016b; NIST., 2018) (Fig. 8a).

BIT166 then oxidizes further, split into two potential pathways. The first pathway involves the same mechanism of radical addition/hydroxylation at the sulfur heteroatom to BIT-SO-OH, a fast unobserved intermediate, subsequently oxidized via $O_2$ to Saccharin (BIT182, a BIT-sulfone). Saccharin has two oxygens attached to the heterocyclic ring's sulfur. The proposed structure is supported by two strong fragments and high mass accuracy (Fig. 8b). The observed accurate mass ($[M-H]^-$: m/z 181.9920, $C_7H_5O_3NS$) is within 1.4 ppm of the theoretical mass.

372 Fragments m/z 118.0300 and m/z 105.9607 are proposed to be due to the loss of $SO_2$ and $C_6H_4$,
373 respectively. The latter fragment shows cleavage down the center of the molecule (Fig. 8b).

374 The second pathway is more radical driven. BIT166 is oxidized via hydroxyl radical reaction
375 (hydroxylating the sulfur heteroatom) and receives a hydrogen on the adjacent nitrogen.
376 Subsequent heterocyclic ring breakage separates the sulfur and nitrogen moieties, forming
377 unobserved intermediates BIT-sulfinic acid (BIT-SA) and hydroxylated BIT-SA (BIT-SA-OH)
378 in succession. This is further oxidized via radical reaction to BIT200, a BIT-sulfonic acid. The
379 proposed structure includes a sulfate moiety that is likely cleaved during further degradation.
380 The mass measurement accuracy for this molecular formula ($[M-H]^-$: m/z 200.0034,
381 $C_7H_7O_4NS$) is 5.5 ppm. The fragment ion m/z 156.9968 is due to cleavage between the
382 aromatic ring and the amide moiety of the TP, and m/z 118.0299 is due to loss of the $HSO_3$
383 group (Fig. 8c).

384 The formation of these three TPs agrees well with the chemistry of sulfur containing
385 compounds subjected to the attack of OH radicals. It is known that the sulfur atom of alkyl
386 sulfide is oxidized by OH radical to sulfoxide and the latter to sulfone and sulfonic acid (Arsene
387 et al. 2002).

388 These three TPs have also been reported in ozonation reactions of benzisothiazolinone,
389 although there are notable mechanistic differences between ozonation and UV/$H_2O_2$
390 degradation. Li et al. (2016b) proposed a transformation pathway for the ozonation degradation
391 of BIT. The addition of oxygen occurs primarily at the electron-rich divalent sulfur in the
392 heterocyclic ring. In this mechanism, BIT is fully degraded to sulfate ions, small organic acids,
393 inorganic carbon, and organic nitrogen. Li et al. (2016b) confirmed the second TP
394 (BIT182/saccharin) via standard comparison, as well as a final degradation product of sulfate
395 (Li et al., 2016b).

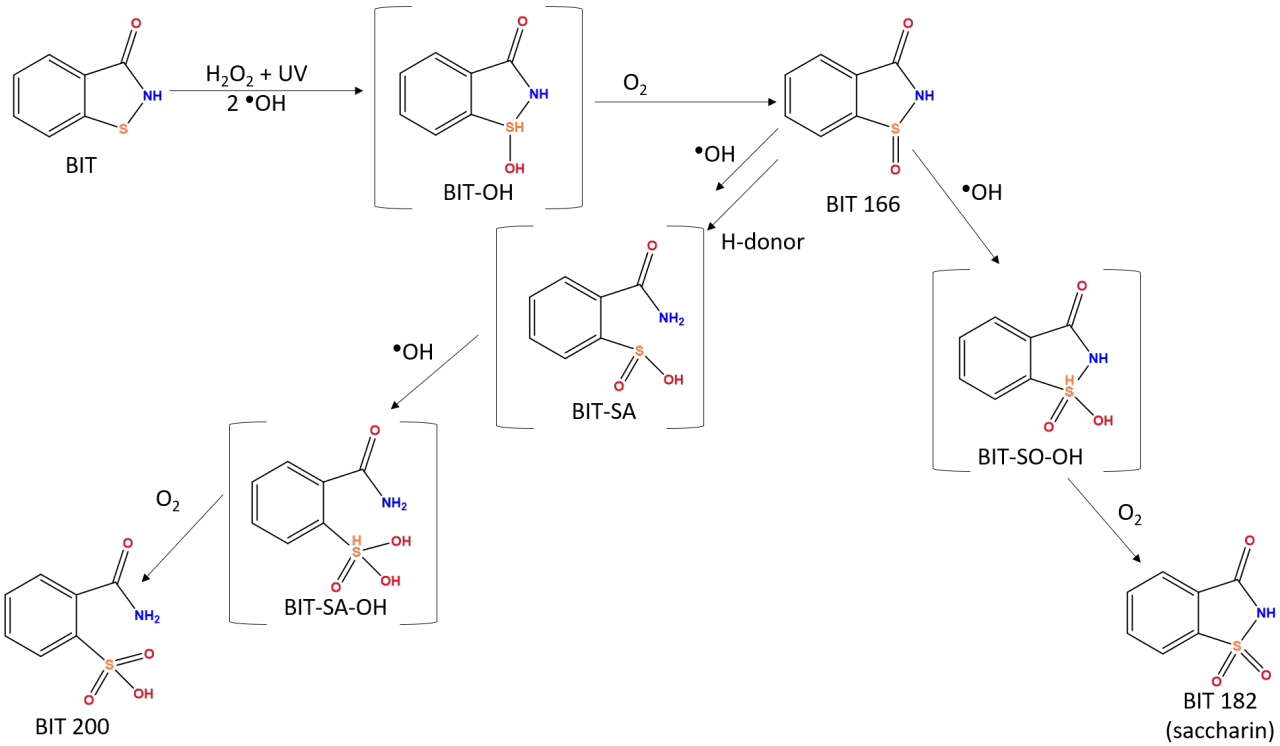


396

397 **Fig. 7.** Proposed mechanistic pathway for UV/$H_2O_2$ advanced oxidation degradation of BIT.

398

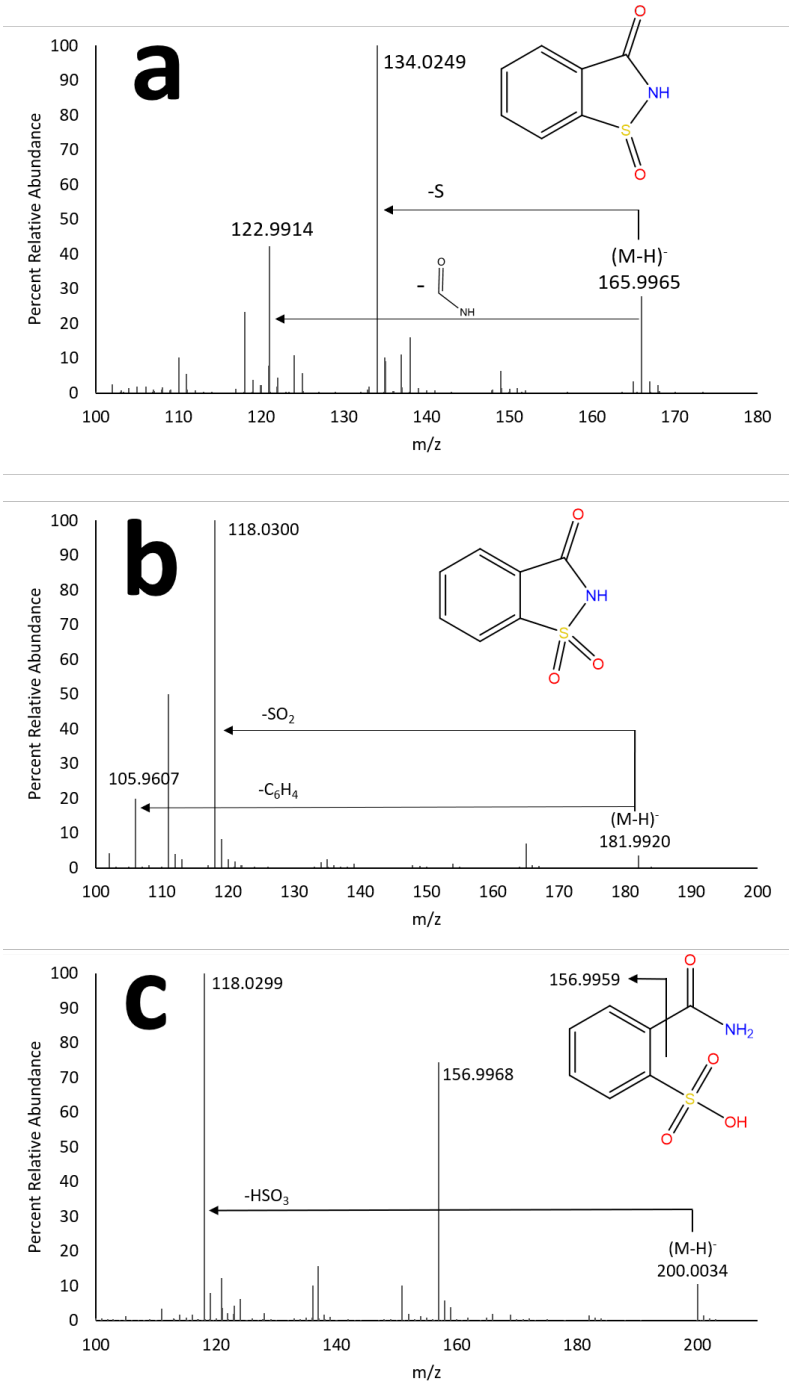


399

400 **Fig. 8.** a) MS/MS spectrum of benzisothiazolinone TP BIT166 with $[M-H]^-$: m/z = 165.9965.
401 b) MS/MS spectrum of benzisothiazolinone TP BIT182 (saccharin) with $[M-H]^-$: m/z =
402 181.9920. c) MS/MS spectrum of benzisothiazolinone TP BIT200 with $[M-H]^-$: m/z =
403 200.0034. For all three transformation products, the scan range was m/z 50-750, but no
404 fragment ions were seen below m/z 100.

## CONCLUSIONS

In this study, the photodegradation of MIT, BIT, and isoxazole by $UV_{254}$ and $UV_{254}/H_2O_2$ processes was investigated in a highly efficient microcapillary photoreactor, which allos rapid investigation of the degradation kinetics.

The collected data were used to develop kinetic models for the estimation of the quantum yields of direct photolysis and the rate constant of reaction with the photogenerated OH radicals. The accuracy of the determined rate constants was demonstrated by predicting the photodegradation of mixtures of the three target compounds in both ultrapure water and in synthetic wastewater. The estimated values are in agreement with those reported in the literature for compounds with a similar molecular structure. In consequence, this study has shown a fast method for determination of water contaminants reactions rate constants which can be of use for the design of advanced water treatment processes. Furthermore, the use of a microphotoreactor allows for the faster identification of the reaction mechanism and of the photo-degradation byproducts. As a result, a mechanistic pathway was proposed for $UV/H_2O_2$ advanced oxidation degradation of BIT, the first such pathway for this treatment of BIT. The main transformation products of BIT photo-degradation proposed in the novel mechanistic pathway were tentatively identified via high resolution accurate mass MS/MS, suggesting the addition of oxygens to the heterocyclic ring

The identification of the key transformation byproducts and the evaluation of the kinetic parameters would allow the further development of complex models that address the degradation of key target compounds in real wastewater matrices, as well as the evaluation of the ecotoxicity of parent compounds and their by-products on aquatic organisms. The ultrafast micro-photoreactor methodology described in this study lays the groundwork for an

environmentally friendly, cost effective, time-saving experimental protocol for studies of homogeneous phase AOPs.

**Acknowledgements**

We would like to acknowledge Agilent Technologies for technical assistance and instrument support. The Authors are grateful to ERASMUS-Mobility Student Program, and to Eng. Francesco Izzo and Marianna Lombardi for their precious support during the experimental campaign.

**References**

Amat, A.M., Arques, A., Lopez-Perez, M.F., Nacher, M., Palacios, S., Effect of methylisothiazolinone on biological treatment: efficiency of SBRs and bioindicative studies, Environmental Engineering Science 32 (2015), 479 – 485.

Andreozzi, R., Marotta, R., Nicklas, P., Pharmaceuticals in STP effluents and their solar photodegradation in aquatic environment, Chemosphere 50 (2003), 1319 – 1330.

Arsene, C., Barnes, I., Becker, K.H., Schneider, W.F., Wallington, T.T., Mihalopoulos, N., Patroescu-Klotz, I.V., Formation of methane sufinic acid in the gas-phase OH-radical initiated oxidation of dimethyl sulfoxide, Environ. Sci. Technol. 36 (2002), 5155 – 5163.

Atkinson, R., Baulch, D.L., Cox, R.A., Hampson, R.F., Kerr, J.A., Rossi, M.J., Troe, J., Evaluated kinetic, photochemical and heterogeneous data for atmospheric chemistry: supplement V. IUPAC subcommittee on gas kinetic data evaluation for atmospheric chemistry, Journal of Phys. and Chem. Ref. Data 26 (1997), 521.

Barnes, I., Becker, K.H., Patroescu, I., FTIR product study of the OH initiated oxidation of dimethyl sulphide: observation of carbonyl sulphide and dimethyl sulphoxide, Atmopheric Environ. 30 (1996), 1805-1814.

Bensalah, N., Chair, K., Bedoui, A., Efficient degradation of tannic acid in water by UV/$H_2O_2$ process, Sustainable Environment Research 28 (2018), 1-11.

Bollman, U.E., Tang, C., Eriksson, E., Jonsson, K., Vollertsen, J., Bester, K., Biocides in urban wastewater treatment plant influent at dry and wet weather: concentrations, mass flow and possible sources, Water Research 60 (2014), 64 – 74.

Clerici, F., Gelmi, M.L., Pellegrino, S., Comprehensive heterocyclic chemistry III, in Chemistry, molecular sciences and chemical engineering, Volume 4, 2008, 545-633.

Daidone, G., Raffa, D., Maggio, B., Plescia, F., Cutuli, V.M.C., Mangano, N.G., Caruso, A., Synthesis and antiproliferative activity of novel 3-(indazol-3-yl)-qui- nazolin-4(3H)-one and (indazol-3-yl)-benzotriazin-4(3H)-one derivatives, Arch. Pharm. Med. Chem. 50 (1999) 332.

Dogan, I., Steenken, S., Schulte-Frohlinde, D., Icli, S., Electron spin resonance and pulse radiolysis studies on the reaction of OH and $SO^{-}_4$ with five-membered heterocyclic compounds in aqueous solutions, Journal of Physical Chemistry 94 (1990), 1887-1894.

Garcia Einschlag, F.S., Carlos, L., Capparelli, A.L., Competition kinetics using the UV/$H_2O_2$ process: a structure reactivity correlation for the rate constants of hydroxyl radicals towards nitroaromatic compounds, Chemosphere 53 (2003) 1-7.

Garcia-Hidalgo, E., Sottas, V., von Goetz, N., Hauri, U., Bogdal, C., Hungerbuhler, K., Occurrence and concentration of isothiazolinones in detergents and cosmetics in Switzerland, Contact Dermatitis (2016).

Geier, J., Lessmann, H., Schnuch, A., Uter, W., Recent increase in allergic reactions to methylchloroisothiazolinone/methylisothiazolinone: is methylisothiazolinone the culprit?, Contact Dermatitis 67 (2012), 334 – 341.

Ghattas, A.K., Fischer, F., Wick, A., Ternes, T.A., Anaerobic biodegradation of (emerging) organic contaminants in the aquatic environment, Water Research 116 (2017), 268-295.

Gribble, G., Joule, J., Progress in Heterocyclic Chemistry, Volume 15, 1st edition, 2003.

Guo, Y., Wang, H., Wang, B., Deng, S., Huang, J., Yu, G., Wang, Y., Prediction of micropollutant abatement during homogeneous catalytic ozonation by a chemical kinetic model, Water Reserach 142 (2018), 383-395.

Hamad, N.M.M., Sharshira, E.M., Synthesis and antimicrobial evaluation of some heterocyclic chalcone derivatives, Molecules 16 (2011), 2304-2312.

Han, W., Chen, Y., Wang, L., Sun, X., Li, J., Mechanism and kinetics of electrochemical degradation of isothiazolin-ones using Ti/SnO2-Sb/PbO2 anode, Desalination 276 (2011), 82 – 88.

Hirsch, R., Ternes, T., Haberer, K., Kratz, K.L., Occurrence of antibiotics in the aquatic environment, Science of The Total Environment 225 (1999), 109 – 118.

Huang, Y., Liu, Y., Kong, M., Xu, E.G., Coffin, S., Schlenk, D., Dionysiou, D.D., Efficient degradation of cytotoxic contaminants of emerging concern by UV/$H_2O_2$, Environmental Science: Water Research & Technology 4 (2108), 1272-1281.

Hynes, A.J., Stoker, R.B., Pounds, A.J., McKay, T., Bradshaw, J.D., Nicovich, J.M., Wine, P.H., A mechanistic study of the reaction of OH with dimethyl-$d_6$ sulfide. Direct observation of adduct formation and the kinetics of the adduct reaction with $O_2$, J. Phys. Chem. 99 (1995), 16967-16975.

Jungnickel, C., Stock, F., Brandsch, T., Ranke, J., Risk assessment of biocides in roof paint. Part 1: experimental determination and modelling of biocide leaching from roof paint. Env. Sci. Pollut. Res. 15 (2008), 258-265.

Kandavelu, V., Kastien, H., Thampi, K.R., Photocatalytic degradation of isothiazolin-3-ones in water and emulsion paints containing nanocrystalline TiO2 and ZnO catalysts, Applied Catalysis B: Environmental 48 (2004), 101 – 111.

Kohanski, M.A., DePristo, M.A., Collins, J.J., Sub-lethal antibiotic treatment leads to multidrug resistance via radical-induced mutagenesis, Molecular Cell 37 (2010), 311-320.

Lado Ribeiro, A.R., Moreira, N.F.F., Li Puma, G., Silva, A.M.T., Impact of water matrix on the removal of micropollutants by advanced oxidation technologies, Chem. Eng. J 363 (2019), 155-173.

Lee, Y.S., Kim, B.H., Heterocyclic nucleoside analogues: design and synthesis of antiviral, modified nucleosides containing isoxazole heterocycles, Bioorganic & Medicinal Chemistry Letters 12 (2002), 1395-1397.

Li, K., Stefan, M.I., Crittenden, J.C., Trichloroethene degradation by UV/$H_2O_2$ advanced oxidation process: product study and kinetic modeling, Environ. Sci. Technol. 41 (2007), 1696-1703.

Li, A., Wu, Q.Y., Tian, G.P., Hu, H.Y., Effective degradation of methylisothiazolone biocide using ozone: kinetics, mechanisms, and decreases in toxicity, Journal of Environmental Management 183 (2016a), 1064 – 1071.

Li, A., Chen, Z., Wu, Q.Y., Huang, M.H., Liu, Z.Y., Chen, P., Mei, L.C., Hu, H.Y., Study on the removal of benzisothiazolinone biocide and its toxicity: the effectiveness of ozonation, Chemical Engineering Journal 300 (2016b), 376 – 383.

Lin, D., Zhou, Q., Xie, X., Liu, Y., Potential biochemical and genetic toxicity of triclosan as an emerging pollutant on earthworms (Eisenia fetida), Chemosphere 81 (2010), 1328-1333.

Liu, W.R., Zhao, J.L., Liu, Y.S., Chen, Z.F., Yang, Y.Y., Zhang, Q.Q., Ying, G.G., biocides in the Yangtze river of China: spatiotemporal distribution, mass load and risk assessment, Environmental Pollution 200 (2015), 53 – 63.

Lugg, M.J., Photodegradation of the biocide 1,2-benziothiazolin-3-one used in a paper-based jointing material, International Biodeterioration & Biodegradation 48 (2001), 252 – 254.

Luo, Y., Guo, W., Ngo, H.H., Nghiem, L.D., Hai, F.I., Zhang, J., Liang, S., Wang, X.C., A review on the occurrence of micropollutants in the aquatic environment and their fate and removal during wastewater treatment, Science of The Total Environment, 473-474 (2014), 619 – 641.

Mack, J., Bolton, J.R., Photochemistry of nitrite and nitrate in aqueous solution: a review, J. Photochem. Photobiol. A 128 (1999), 1-13.

Maczynski, M., Artym, J., Kocieba, M., Kochanowska, I., Rying, S., Zimecki, M., Anti-inflammatory properties of an isoxazole derivative – MZO-2, Parmacol. Rep. 68 (2016), 894 – 902.

Margot., J., Rossi, L., Barry, D.A., Holliger, C., A review of the fate of micropollutants in wastewater treatment plants, WIREs Water 2 (2015), 457 – 487.

McCance, W., Jones, O.A.H., Edwards, M., Surapaneni, A., Chadalavada, S., Currell, M., Contaminants of emerging concern as novel groundwater tracers for delineating wastewater impacts in urban and peri-urban areas, Water Research 146 (2018), 118-133.

Miraji, H., Othman, O.C., Ngassapa, F.N., Mureithi, E.W., Research trends in emerging contaminants on the aquatic environments of Tanzania, Scientifica (2016).

Nicole, I., De Laat, J., Doré, M., Duguet, J.P., Bonnel, C., Use of UV radiation in water treatment: measurement of photonic flux by hydrogen peroxide actinometry, Water Research 24 (1990), 157 – 168.

NIST, Dibenzothiophene, 5-oxide, Gaithersburg, MD, 2018. https://webbook.nist.gov/cgi/inchi?ID=C1013236&Mask=200.

589 Organisation for Economic Cooperation and development (OECD), Guidelines for the
590 Testing of Chemicals, Section 2, 2008, 202.
591
592 Ramirez-Anguita, J.M., Gonzalez-Lafont, A., Lluch, J.M., Formation pathways of DMSO
593 from DMS-OH in the presence of $O_2$ and $NO_x$: a theoretical study, J. Comput. Chem. 30
594 (2008), 173-182.
595
596 Reis, N.M., Li Puma, G., Novel microfluidics approach for extremely fast and efficient
597 photochemical tranformations in fluoropolymer microcapillary films, Chemical
598 Communications, 51 (2015), 8414-8417.
599
600 Russo, D., Spasiano, D., Vaccaro, M., Andreozzi, R., Li Puma, G., Reis, N.M., Marotta, R.,
601 Direct photolysis of benzoylecgonine under UV irradiation at 254 nm in a continuous flow
602 microcapillary array photoreactor, Chemical Engineering Journal 283 (2016), 243 – 250.
603
604 Schriks, M., Heringa, M.B., van der Kooi, M.E., de Voogt, P., van Wezel, A.P.,
605 Toxicological relevance of emerging contaminants for drinking water quality, Water
606 Research 44 (2010), 461 – 476.
607
608 Russo, D., Siciliano, A., Guida, M., Galdiero, E., Amoresano, A., Andreozzi, R., Reis, N.M.,
609 Li Puma, G., Marotta, R., Photodegradation and ecotoxicology of acyclovir in water under
610 $UV_{254}$ and $UV_{254}/H_2O_2$ processes, Water Research 122 (2017), 591 – 602.
611
612 Russo, D., Siciliano, A., Guida, M., Andreozzi, R., Reis, N.M., Li Puma, G., Marotta, R.,
613 Removal of antiretroviral drugs stavudine and zidovudine in water under $UV_{254}$ and
614 $UV_{254}/H_2O_2$ processes: quantum yields, kinetics and ecotoxicology assessment, Journal of
615 Hazardous Materials 349 (2018), 195 – 204.
616
617 Sagi, G., Csay, T., Szabo, L., Patzay, G., Csonka, E., Takacs, E., Wojnarovits, L., Analytical
618 approaches to the OH radical induced degradation of sulfonamide antibiotics in dilute
619 aqueous solutions, Journal of Pharmaceutical and Biomedical Analysis 106 (2015), 52-60.
620
621 Shi, H., Cheng, X., Wu, Q., Mu, R., Ma, Y., Assessment and removal of emerging water
622 contaminants, Environmental & Analytical Toxicology 2(2012).

Siciliano, A., Russo, D., Spasiano, D., Marotta, R., Race, M., Fabbricino, M., Galdiero, E., Guida, M., Chronic toxicity of treated and untreated aqueous solutions containing imidazole-based ionic liquids and their oxydized by-products, Ecotoxicology and Environmental Safety 180 (2019), 466-472.

Spasiano, D., Russo, D., Vaccaro, M., Siciliano, A., Marotta, R., Guida, M., Reis, N.M., Li Puma, G., Andreozzi, R., Removal of benzoylecgonine from water matrices through $UV_{254}/H_2O_2$ process: reaction kinetic modeling, ecotoxicity and genotoxicity assessment, Journal of Hazardous Materials 318 (2016 a), 515 – 525.

Spasiano, D., Siciliano, A., Race, M., Marotta, R., Guida, M., Andreozzi, R., Biodegradation, ecotoxicity and $UV_{254}/H_2O_2$ treatment od imidazole, 1-methyl-imidazole and N,N'-alkyl-imidazolium chlorides in water, Water Research 106 (2016 b), 450-460.

Speksnijder, P., van Ravestijn, J., de Voogt, P., Trace analysis of isothiazolinones in water samples by large-volume direct injection liquid chromatography tandem mass spectrometry, Journal of Chromatography A, 1217 (2010), 5184 – 5189.

Srivastava, S., Bajpai, L.K., Batra, S., Bhaduri, A.P., Maikhuri, J.P., Gupta, G., Dhar, J.D., In search of new chemical entities with spermicidal and anti-HIV activities, Bioorganic & Medicinal Chemistry 7 (1999), 2607 – 2613.

Stamm, C., Eggen, R.I.L., Hering, J.G., Hollender, J., Joss, A., Scharer, M., Micropollutant removal from wastewater: facts and decision-making despite uncertainty, Environmental Science & Technology 49 (2015), 6374 – 6375.

Tanji, Y., Nishihara, T., Miyanaga, K., Iron dependent degradation of an isothiazolone biocide (5-chloro-2-methyl-isothiazolin-3-one), Biofouling 23 (2007), 73 – 77.

Van Huizen, A.V., Tseng, A.S., Beane, W.S., Methylisothiazolinone toxicity and inhibition of wound healing and regeneration in planaria, Aquatic Toxicology 191 (2017), 226 – 235.

Vicentini, C.B., Romagnoli, C., Manfredini, S., Rossi, D., Mares, D., Pyrazolo[3,4-c]isothiazole and isothiazolo[4,3-d]isoxazole derivatives as antifungal agents, Pharmaceutical Biology 49 (2011), 545 – 552.

Wanda, E.M.M., Nyoni, H., Mamba, B.B., Msagati, T.A.M., Occurrence of emerging micropollutants in water systems in Gauteng, Mpumalanga, and north west provinces, South Africa, Int. J. Environ. Res. Public Health (2017), 14, 79.

Wang., T., Wu, Q.Y., Wang, W.L., Chen, Z., Li, B.T., Li, A., Liu, Z.Y., Hu, H.Y., Self-sensitized photodegradation of benzisothiazolinone by low-pressure UV-C irradiation: kinetics, machanisms, and the effect of media, Separation and Purification Technology 189 (2017), 419 – 424.

Wieck, S., Olsson, O., Kummerer, K., Possible underestimation of risks for the environment due to unregulated emissions of biocides from households to wastewater. Environmental International 94 (2016), 695 – 705.

Wine, P.H., Kreutter, N.M., Gump, C.A., Ravishankara, A.R., Kinetics of OH reactions with the atmospheric sulfur compounds $H_2S$, $CH_3SH$, $CH_3SCH_3$, and $CH_3SSCH_3$, J. Phys. Chem. 85 (1981), 2660-2665.

Yong, J.P., Lu, C.Z., Wu, X., Potential anticancer agents. I. Synthesis of isoxazole moiety containing quinazoline derivatives and preliminarily in vitro anticancer activity, Anti-Cancer Agents in Medicinal Chemistry 15 (2015), 131 – 136.

Zhang, N.S., Liu, Y.S., Van de Brink, P.J., Price, O.R., Ying, G.G., Ecological risks of home and personal care products in the riverine environment of a rural region in South China without domestic wastewater treatment facilities, Ecotoxicology and Environmental Safety 122 (2015), 417 – 425.

Zimecki, M., Bachor, U., Maczynski, M., Isoxazole derivatives as regulators of immune functions, Molecules 23 (2018), 2724.

# Supplementary Information

# Ultrafast photodegradation of isoxazole and isothiazolinones by $UV_{254}$ and $UV_{254}/H_2O_2$ photolysis in a microcapillary reactor

Danilo Russo[a,d*], Kristin H. Cochran[b], Danielle Westerman[b], Gianluca Li Puma[c], Raffaele Marotta[d], Roberto Andreozzi[d], Susan D. Richardson[b,*].

[a] Present address: Department of Chemical Engineering and Biotechnology, University of Cambridge, UK.

[b] Department of Chemistry and Biochemistry, University of South Carolina, USA.

[c] Environmental Nanocatalysis & Photoreaction Engineering, Department of Chemical Engineering, Loughborough University, UK.

[d] Dipartimento di Ingegneria Chimica, dei Materiali e della Produzione Industriale, Università di Napoli Federico II, Italy.

*Corresponding author: Danilo Russo: danilo.russo3@unina.it; dr473@cam.ac.uk; Susan D. Richardson, RICHA545@mailbox.sc.edu.

Keywords: micropollutants; advanced oxidation processes; isoxazole; water reclamation; water treatment; isothiazolinones.

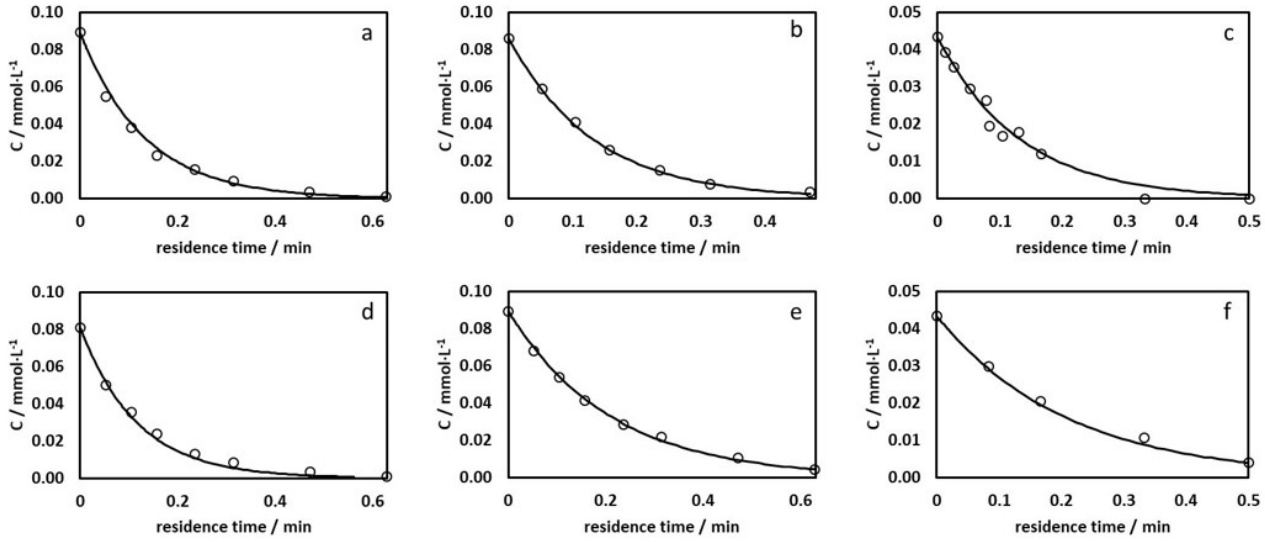


710

711 **Fig. S1.A.** Direct photolysis of MIT. Experimental data (○), calculated data (curves).

712 Experimental conditions are reported in Table S1.

713

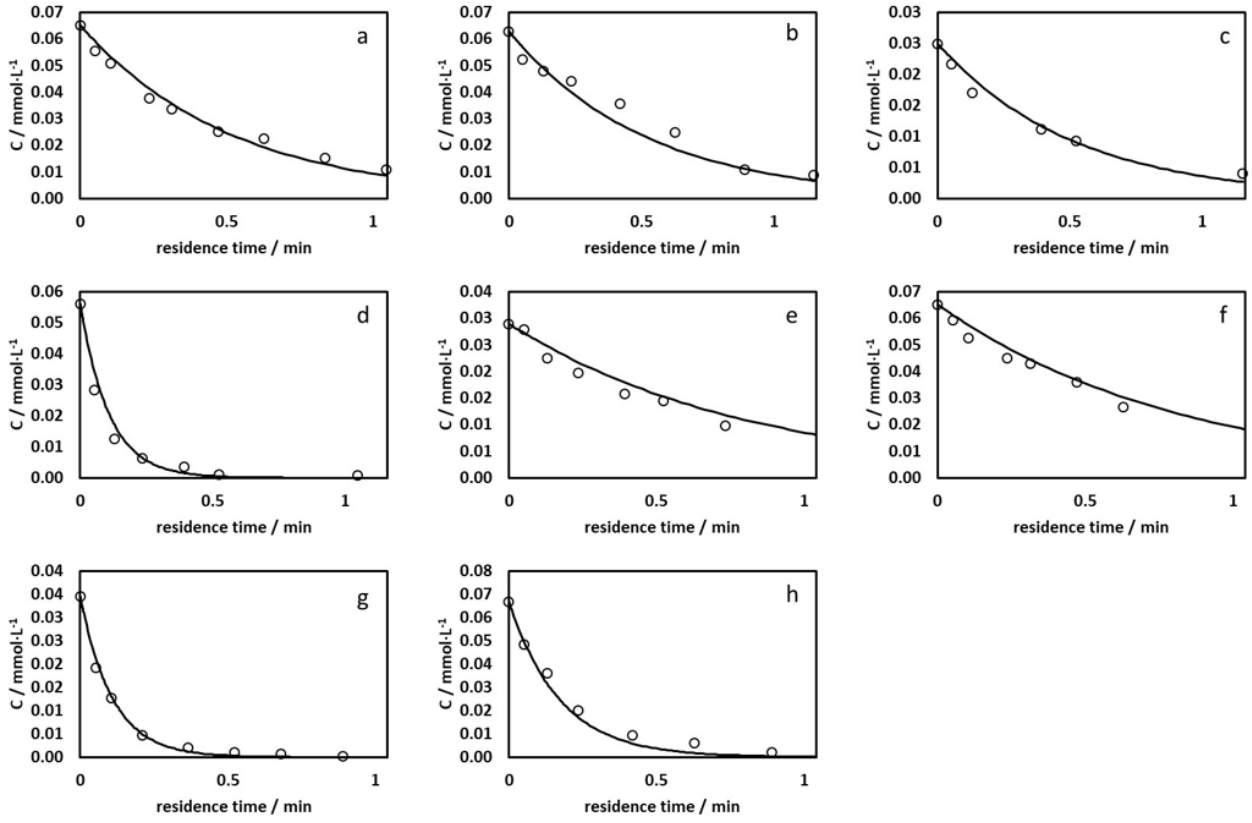


714

715 **Fig. S1.B.** Direct photolysis of BIT. Experimental data (○), calculated data (curves).

716 Experimental conditions are reported in Table S1.

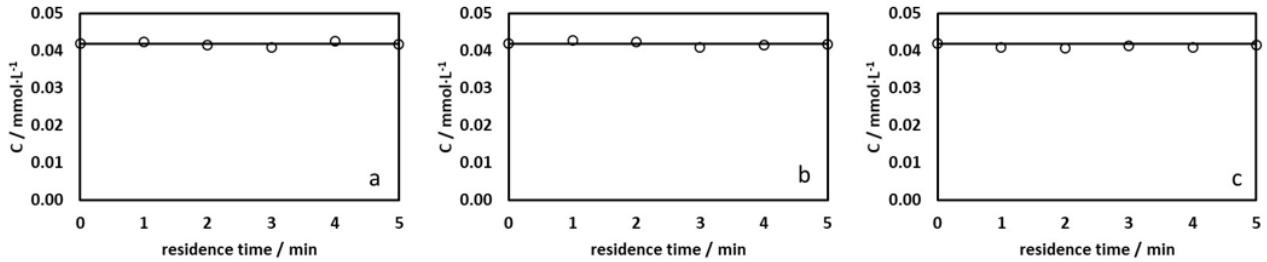


**Fig. S1.C.** Direct photolysis of ISOX. Experimental data (○), calculated data (curves). Experimental conditions are reported in Table S1.

Table S1. Experimental conditions adopted for quantum yield estimation. σ (%) is the overall percentage standard deviation.

| Reference Fig. S1 | Compounds | $[S_i]_0$ (mmol·L$^{-1}$) | pH | Nominal P (W) | σ (%) |
|---|---|---|---|---|---|
| A-a | MIT | 0.0894 | 6 | 8.0 | 1.37 |
| A-b | MIT | 0.0862 | 4 | 8.0 | 0.43 |
| A-c | MIT | 0.0434 | 6 | 8.0 | 0.15 |
| A-d | MIT | 0.0809 | 8 | 8.0 | 0.49 |
| A-e | MIT | 0.0809 | 6 | 4.5 | 0.27 |
| A-f | MIT | 0.0434 | 6 | 4.5 | 1.16 |
| B-a | BIT | 0.0653 | 6 | 8.0 | 1.61 |
| B-b | BIT | 0.0630 | 4 | 8.0 | 1.62 |
| B-c | BIT | 0.0250 | 6 | 8.0 | 0.88 |
| B-d | BIT | 0.0562 | 8 | 8.0 | 2.48 |
| B-e | BIT | 0.0290 | 6 | 4.5 | 1.13 |
| B-f | BIT | 0.0653 | 6 | 4.5 | 2.12 |
| B-g | BIT | 0.0346 | 8 | 8.0 | 2.54 |

| | | | | | |
|---|---|---|---|---|---|
| B-h | BIT | 0.0669 | 8 | 4.5 | 1.80 |
| C-a | ISOX | 0.0420 | 4 | 8.0 | / |
| C-b | ISOX | 0.0420 | 6 | 8.0 | / |
| C-c | ISOX | 0.0420 | 8 | 8.0 | / |

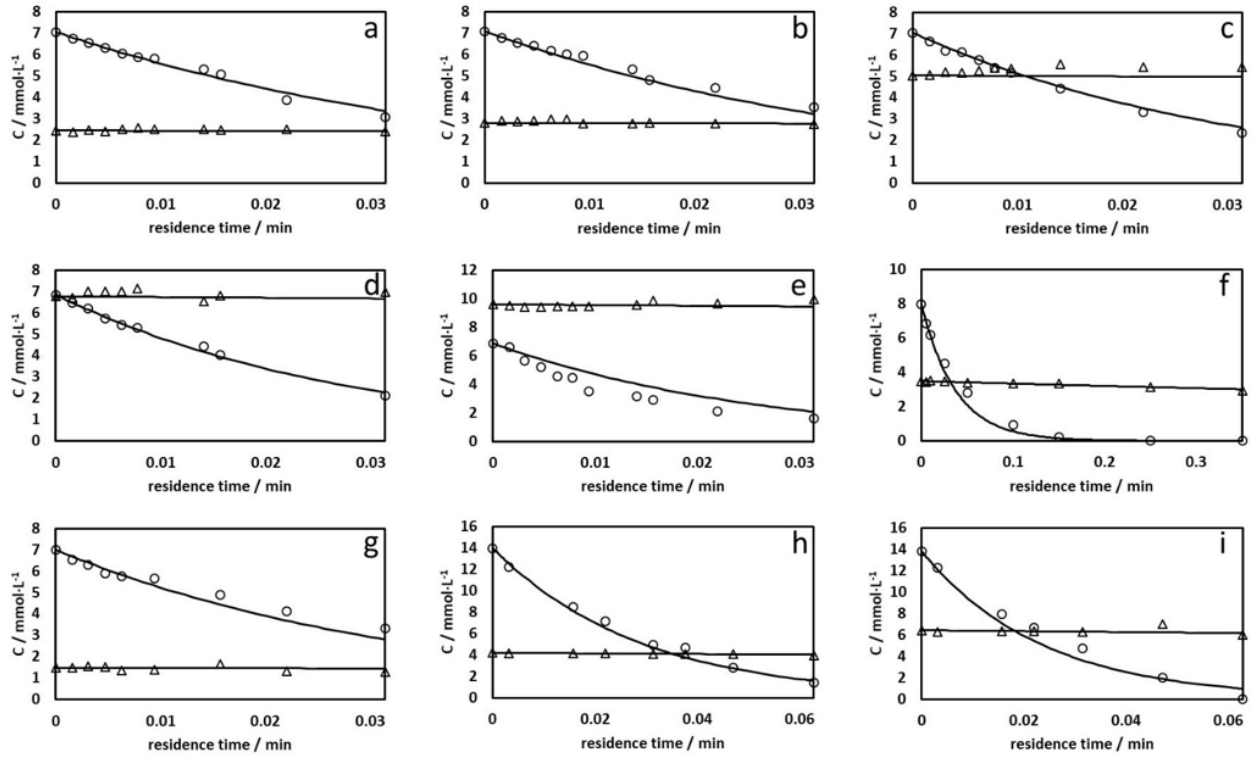


**Fig. S2.A.** Photodegradation of MIT by $UV_{254}/H_2O_2$.in MilliQ water: experimental data (symbols), calculated data (lines). MIT (○), $H_2O_2$ (Δ). MIT concentrations are multiplied by 160 for viewing convenience.

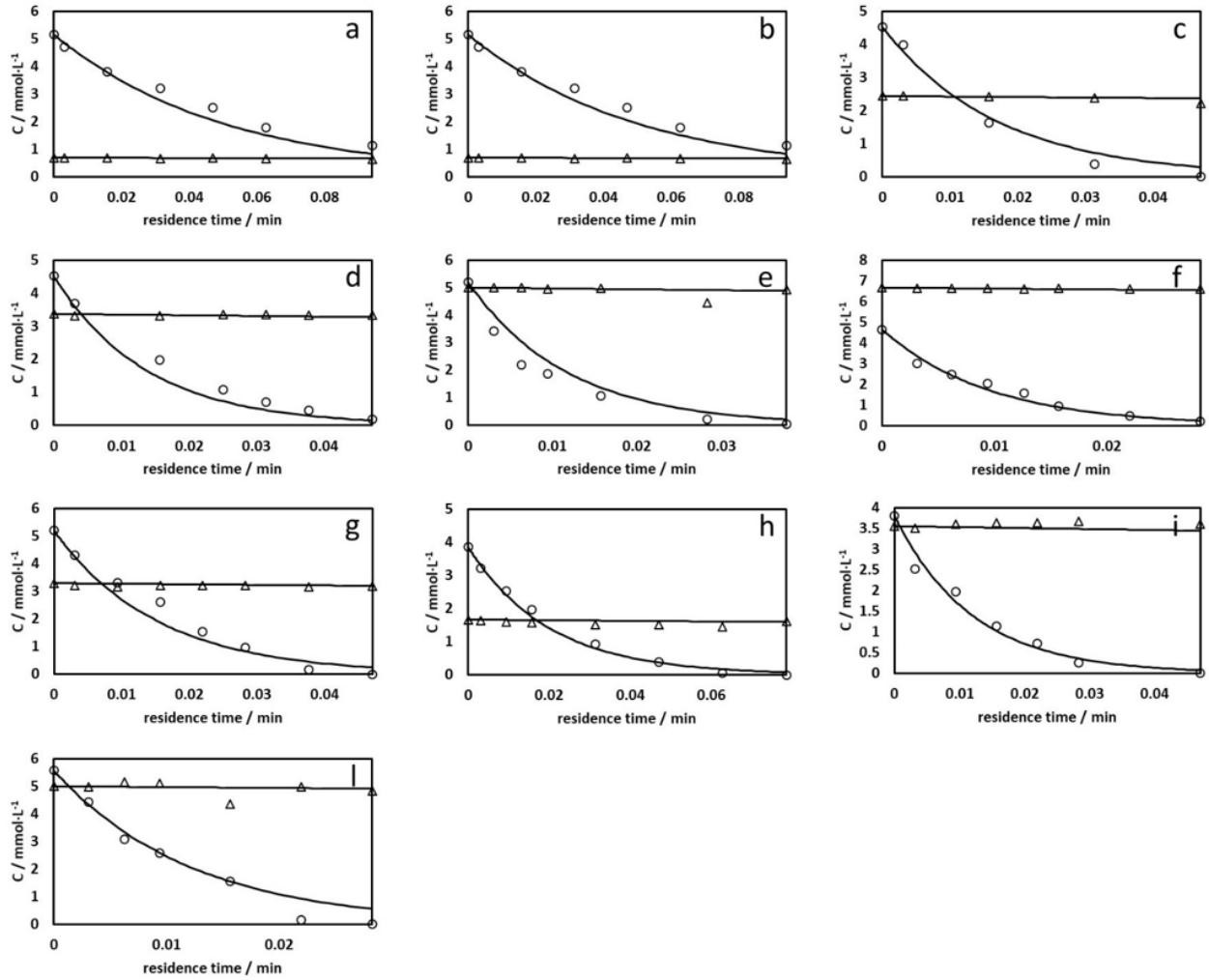


733

734 **Fig. S2.B.** Photodegradation of BIT by $UV_{254}/H_2O_2$.in MilliQ water: experimental data

735 (symbols), calculated data (lines). BIT (○), $H_2O_2$ (Δ). BIT concentrations are multiplied by

736 160 for viewing convenience.

737

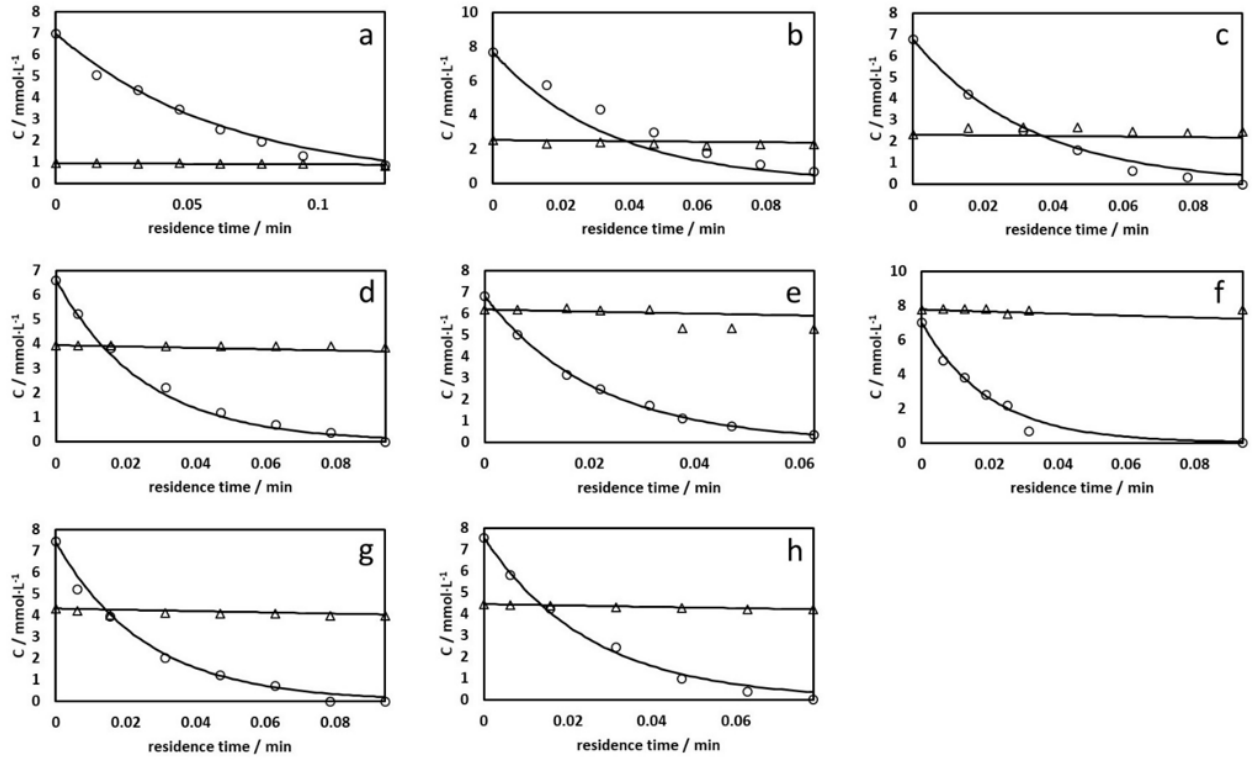


738

739 **Fig. S2.C.** Photodegradation of ISOX by $UV_{254}/H_2O_2$.in MilliQ water: experimental data

740 (symbols), calculated data (lines). ISOX (○), $H_2O_2$ (Δ). ISOX concentrations are multiplied

741 by 160 for viewing convenience.

742

743

744 Table S2. Experimental conditions adopted for $k_{HO}^{i}$ estimation. σ (%) is the overall

745 percentage standard deviation.

| Reference Fig. S2 | Compounds | $[S_i]_0$ (mmol·L$^{-1}$) | $[H_2O_2]_0$ (mmol·L$^{-1}$) | pH | Nominal P (W) | σ (%) |
|---|---|---|---|---|---|---|
| A-a | MIT | 0.044 | 2.45 | 6 | 4.5 | 0.95 |
| A-b | MIT | 0.044 | 2.82 | 6 | 4.5 | 0.79 |
| A-c | MIT | 0.044 | 5.04 | 6 | 4.5 | 1.68 |
| A-d | MIT | 0.043 | 6.77 | 6 | 4.5 | 2.12 |
| A-e | MIT | 0.043 | 9.60 | 6 | 4.5 | 3.39 |

| | | | | | | |
|---|---|---|---|---|---|---|
| A-f | MIT | 0.050 | 3.49 | 8 | 4.5 | 0.73 |
| A-g | MIT | 0.044 | 1.48 | 6 | 8.0 | 0.63 |
| A-h | MIT | 0.088 | 4.20 | 6 | 8.0 | 0.80 |
| A-i | MIT | 0.086 | 6.44 | 6 | 8.0 | 2.44 |
| B-a | BIT | 0.032 | 0.69 | 6 | 8.0 | 2.00 |
| B-b | BIT | 0.032 | 1.57 | 6 | 8.0 | 3.38 |
| B-c | BIT | 0.028 | 2.44 | 6 | 8.0 | 1.25 |
| B-d | BIT | 0.028 | 3.37 | 6 | 8.0 | 2.21 |
| B-e | BIT | 0.033 | 5.00 | 6 | 8.0 | 4.73 |
| B-f | BIT | 0.029 | 6.68 | 6 | 8.0 | 0.34 |
| B-g | BIT | 0.033 | 3.30 | 4 | 8.0 | 2.98 |
| B-h | BIT | 0.024 | 1.67 | 8 | 8.0 | 2.24 |
| B-i | BIT | 0.024 | 3.56 | 8 | 8.0 | 1.64 |
| B-l | BIT | 0.035 | 5.01 | 8 | 8.0 | 0.55 |
| C-a | ISOX | 0.044 | 0.93 | 6 | 8.0 | 1.29 |
| C-b | ISOX | 0.048 | 2.55 | 6 | 8.0 | 6.22 |
| C-c | ISOX | 0.042 | 2.32 | 6 | 8.0 | 4.91 |
| C-d | ISOX | 0.041 | 3.95 | 6 | 8.0 | 1.77 |
| C-e | ISOX | 0.043 | 6.20 | 6 | 8.0 | 1.33 |
| C-f | ISOX | 0.040 | 7.77 | 6 | 8.0 | 1.22 |
| C-g | ISOX | 0.047 | 4.33 | 8 | 8.0 | 2.24 |
| C-h | ISOX | 0.047 | 4.46 | 4 | 8.0 | 0.49 |

746

747